Thermal exchange bias field drift in field cooled Mn 83 Ir 17 / Co 70 Fe 30 thin films after 10 keV He ion bombardment

Arno Ehresmann, Christoph Schmidt, Tanja Weis, and Dieter Engel

Advertisement:
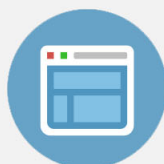
Thermal exchange bias field drift in field cooled Mn$_{83}$Ir$_{17}$/Co$_{70}$Fe$_{30}$ thin films after 10 keV He ion bombardment

Arno Ehresmann,[a)] Christoph Schmidt, Tanja Weis, and Dieter Engel

Institute of Physics and Center for Interdisciplinary Nanostructure Science and Technology (CINSaT),
University of Kassel, Heinrich-Plett-Str. 40, 34132 Kassel, Germany

The thermal exchange bias field drift of sputter deposited Mn$_{83}$Ir$_{17}$(15 nm)/Co$_{70}$Fe$_{30}$(10 nm)/Ta thin films at room temperature after 10 keV He$^+$ ion bombardment in an externally applied in-plane magnetic field for different ion fluences was studied. Although field cooling of the layer system resulted in a temporally stable exchange bias field at room temperature the exchange bias field starts to drift after ion bombardment like in non-annealed samples. Between 1 and 648 h after ion bombardment a logarithmic increase in the absolute magnitude of the exchange bias field is observed. A tentative model is presented for its description based on noninteracting domains in the antiferromagnet. A comparison between experimental data and the model reveals the delicate interplay between the ion bombardment modified average antiferromagnetic anisotropy constants, exchange coupling constants, and relaxation time distributions in the polycrystalline layer system influencing the thermal drift velocities. © *2011 American Institute of Physics.*
[doi:10.1063/1.3532046]

I. INTRODUCTION

Antiferromagnet/ferromagnet thin film systems showing exchange bias (EB)[1,2] play an important role in technical applications, e.g., when pinning the magnetization of the ferromagnetic reference electrode of magnetoresistive sensors.[3,4] Therefore the EB and coercive fields (H$_{EB}$,H$_C$) must be temporally stable within the temperature range of use. Several polycrystalline EB layer systems, however, showed temporal changes in the EB field after their preparation by field growth (FG),[5,6] where the ferromagnetic layer is deposited first and the antiferromagnetic layer is deposited within a magnetic field. For such systems H$_{EB}$ is usually stabilized by subsequent annealing after FG. Alternatively EB is initialized by field cooling (FC) after layer deposition, where the layer system is heated above the blocking temperature and subsequently cooled down below it inside an applied in-plane magnetic field. By these measures (annealing or FC) usually temporally stable coercive and EB fields are obtained, for some layer systems after training.[7]

Recently it has been shown that this stable EB field may be tailored by keV He ion bombardment (IB) in an applied magnetic field in magnitude and direction (Refs. 8 and 9 and references therein). It has been shown that this technique is useful for setting the pinning direction of the magnetic reference electrode in giant magnetoresistance layer stacks[10] and in magnetic tunnel junctions based on AlO$_x$ tunnel layers[11,12] after layer deposition and EB initialization almost without reducing the magnetoresistive effect amplitude. However, first evidences have been found[9] that the originally stable EB starts to drift after the IB, resembling the thermal after effect of nonannealed samples.[6] Therefore the current paper is a first systematic investigation of the thermal EB field drift after keV He ion bombardment of EB bilayers,

here for MnIr/CoFe layer systems. The effect will be modeled by assuming noninteracting antiferromagnetic grains in a polycrystalline layer based on ideas of Refs. 5, 13, and 14. The model is in qualitative agreement with recent studies (Ref. 15 and references therein) and stresses the importance of antiferromagnetic anisotropy constant, exchange coupling constant, grain volume, and grain geometry distributions for the description of EB in polycrystalline layers.

II. EXPERIMENT

A. Sample preparation

The Mn$_{83}$Ir$_{17}$(15 nm)/Co$_{70}$Fe$_{30}$(10 nm)/Ta(3 nm) films were deposited by rf-sputtering onto a naturally oxidized Si(100) substrate with a buffer layer of 50 nm Cu and then broken into pieces of 15×10 mm^2. The base pressure was 8.0×10^{-6} mbar and the Ar pressure during deposition was 1.5×10^{-2} mbar [Ar flow of 80.1 sccm (sccm denotes cubic centimeter per minute at STP)]. The EB has been initialized by FC of the samples in an in-plane magnetic field of H$_{FC}$=40 kA/m. After heating to 275 °C for 60 min in vacuum (2.5×10^{-6} mbar) they were cooled down to room temperature within 20 min. A magneto optical Kerr effect magnetometer in longitudinal geometry (L-MOKE) was used to characterize the sample's magnetization reversal. The in-plane magnetic field range during characterization was ± 28 kA/m. Before IB the temporal stability of the EB and coercive fields H$_{EB}$ and H$_C$ have been verified by sample storage (a) without an applied magnetic field and (b) in an applied field of 80 kA/m both parallel and antiparallel to the direction of $\vec{H}_{FC}$. H$_{EB}$ and H$_C$ prior to bombardment were constant in all conditions over 30 days. The exchange bias (H$_{EB,0}$) and coercive fields (H$_{C,0}$) of the used samples prior to IB (index 0) were approximately 12.8 kA/m and 5.5 kA/m, respectively.
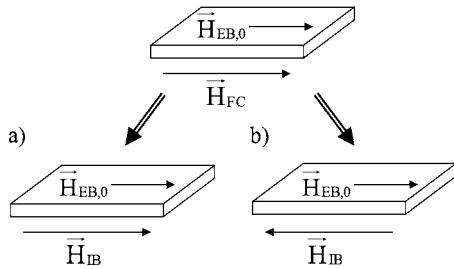
a)Electronic mail: ehresmann@physik.uni-kassel.de.

FIG. 1. Sketch of the two magnetic field geometries during IB ($\vec{H}_{FC}$ =magnetic field during FC; $\vec{H}_{EB,0}$=direction of the initial unidirectional anisotropy after preparation before IB; $\vec{H}_{IB}$=magnetic field during IB): (a) parallel field geometry: $\vec{H}_{FC}\uparrow\uparrow\vec{H}_{IB}$; (b) antiparallel field geometry: $\vec{H}_{FC}\uparrow\downarrow\vec{H}_{IB}$.

B. Modification by ion bombardment

The EB samples were bombarded by 10 keV He$^+$ ions with selected fluences F in the range between 10^{13} and 10^{16} ions/cm^2. The in-plane magnetic field H_{IB}=80 kA/m during IB was oriented *parallel* to the field direction during field cooling $\vec{H}_{FC}$ for samples series 1 and *antiparallel* for samples series 2. The direction of $\vec{H}_{FC}$ is assumed to be parallel to the direction of $\vec{H}_{EB,0}$ (see Fig. 1 for the different bombardment geometries). The areas bombarded with constant fluences were limited to squares $(2\times2$ mm^2) by shadow masks. The distances between bombarded squares were set to 1 mm to rule out interactions between the different bombarded areas. Samples were transported from the IB stage and inserted into the L-MOKE apparatus. The first hysteresis loop has been measured 60 min after IB. Between the characterization measurements no external magnetic field acted on the samples. After one day the interval between L-MOKE characterization measurements has been increased. Bombardment and characterization of the samples have been performed at room temperature.

III. RESULTS

Figure 2 shows a typical result of $H_{EB}(t)$ of the present measurements for a sample bombarded by 1×10^{14} ions/cm^2 for the two field geometries (see Fig. 1), and for a sample area not bombarded by ions. All values determined for H_{EB} from the hysteresis loop measurements have been normalized for the initial EB field before bombardment ($H_{EB,0}$). At t=0 h the sample is still not bombarded and the graph starts at $H_{EB}(t=0$ h$)/H_{EB,0}=1.0$ (open diamond in Fig. 2). Bombardment in parallel field geometry (filled circles) leads to an enhancement of the EB field determined from the hysteresis loop measured 1 h after bombardment (see Sec. II) to $H_{EB}(t=1$ h$)/H_{EB,0}=1.33$. As is obvious from Fig. 2 the subsequent temporal change in H_{EB} is toward larger absolute magnitude and reaches a value of $H_{EB}(t=648$ h$)/H_{EB,0}=1.47$ after 648 h (the end of the present measurements). This corresponds to an absolute H_{EB} increase of 1.78 kA/m compared to the absolute value of H_{EB} determined 1 h after bombardment. The H_{EB} increase with time is approximately logarithmic, similar to observations of the thermal after effect in nonannealed samples.[6]
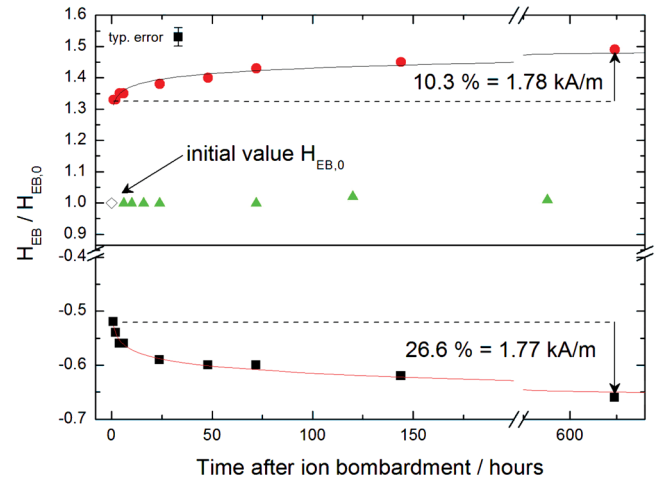

FIG. 2. (Color online) Time dependence of H_{EB} after IB by 1.0×10^{14} ions/cm^2 in the parallel (filled circles) and antiparallel (filled squares) field geometry. The unbombarded reference area (filled triangles) on the same sample remains stable. The initial value (open diamond) corresponds to $H_{EB,0}=12.8$ kA/m. Solid lines are fits with Eq. (1).

One area of the sample remained unbombarded (cf. Fig. 2, filled triangles) and has been used as reference. There, H_{EB} does not change, demonstrating (1) the thermal stability of $H_{EB,0}$ and (2) the negligible interaction between different bombarded areas on the same sample. The filled squares of Fig. 2 display the results of $H_{EB}(t)$ after bombardment in antiparallel field geometry. As expected[8,16] bombardment by 1.0×10^{14} ions/cm^2 results in an EB field directed antiparallel to the original one. For the present sample the normalized EB field amounts to $H_{EB}(t=1$ h$)/H_{EB,0}=-0.52$. Also here a subsequent temporal change is observed, leading to an EB of $H_{EB}(t=648$ h$)/H_{EB,0}=-0.66$. This corresponds to an increase of the absolute EB field of 1.77 kA/m compared to the field determined 1 h after bombardment. Again here the time dependence is logarithmic in the time interval of the measurements.

In Figs. 3 and 4 the experimentally determined
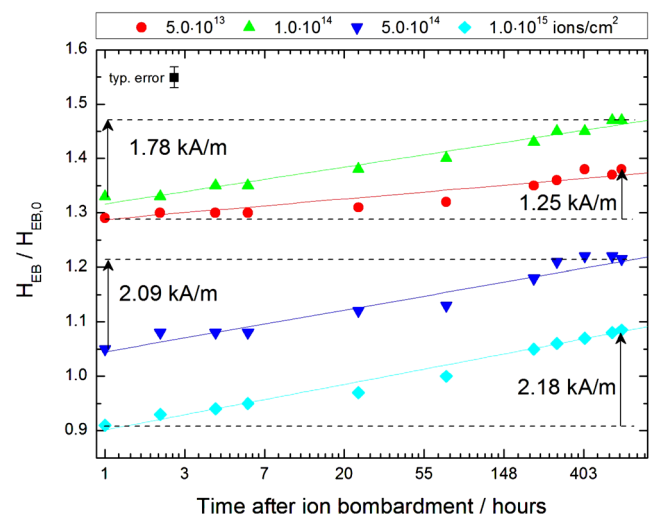

FIG. 3. (Color online) $H_{EB}(t)$ after IB in *parallel* field geometry after bombardment by different ion fluences. The initial value prior to bombardment corresponds to $H_{EB,0}=12.8$ kA/m. Solid lines are fits by Eq. (1).
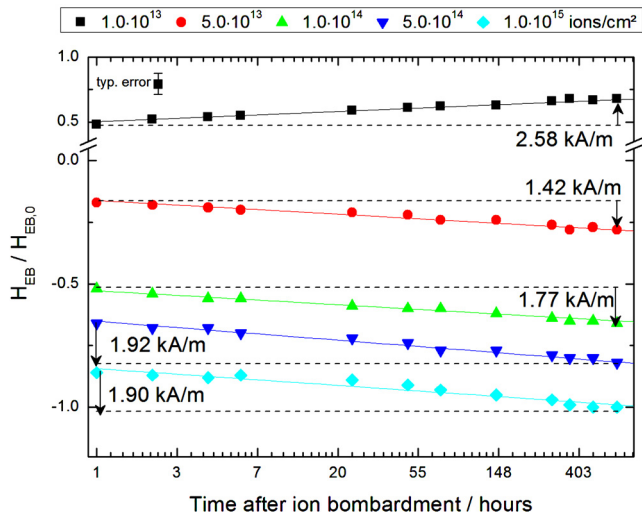
FIG. 4. (Color online) $H_{EB}(t)$ after IB in *antiparallel* field geometry after bombardment by different ion fluences. The initial value prior to bombardment corresponds to $H_{EB,0}=12.8$ kA/m. Solid lines are fits by Eq. (1).

TABLE I. Experimental results and fit coefficients h and Δh for the results displayed in Figs. 3 and 4 according to Eq. (1) for the time dependence of H_{EB} after IB with the given fluences. ΔH_{EB} corresponds to $H_{EB}(t=648$ h) $-H_{EB}(t=1$ h).

Geometry	Ion fluence (ions/cm^2)	ΔH_{EB} (kA/m)	h [1]	Δh (hours^{-1})
Parallel	1.0×10^{13}	1.23	1.193 68	0.010 58
	5.0×10^{13}	1.25	1.287 75	0.012 65
	1.0×10^{14}	1.78	1.316 33	0.022 62
	5.0×10^{14}	2.09	1.044 85	0.025 60
	1.0×10^{15}	2.18	0.901 35	0.027 92
	5.0×10^{15}	1.19	0.305 74	0.016 83
Antiparallel	1.0×10^{13}	2.58	0.496 83	0.028 04
	5.0×10^{13}	−1.42	−0.165 72	−0.016 81
	1.0×10^{14}	−1.77	−0.524 67	−0.019 18
	5.0×10^{14}	−1.92	−0.655 10	−0.022 17
	1.0×10^{15}	−1.90	−0.840 11	−0.025 82
	5.0×10^{15}	−0.68	−0.153 46	−0.005 74

$H_{EB}(t)/H_{EB,0}$ obtained after bombardment by different ion fluences F are shown on logarithmic time scale for both the parallel and antiparallel field geometry, respectively.

As is evident from Fig. 5 the values of $H_{EB}(t=1$ h$)/H_{EB,0}$ and of $H_{EB}(t=648$ h$)/H_{EB,0}$ as a function of the ion fluence in the different field geometries are qualitatively consistent with the results of the determined fluence dependencies of other exchange biased layer systems.[8,16,17] The temporal change in the EB field at room temperature always tends to increase the absolute magnitude of the EB field *after bombardment*. This is obvious particularly from Fig. 4, where the fluence of 1×10^{13} ions/cm^2 is not sufficient to reverse the sign of the EB field when bombarding in antiparallel field geometry, in contrast to the higher fluences.

As outlined in the model considerations below the experimental results have been fitted by

$$H_{EB}(t)/H_{EB,0} = h + \Delta h \ln(t) \qquad (1)$$

with two free fit parameters [$h=H_{EB}(t=1$ h$)/H_{EB,0}$ and Δh]. The corresponding fit lines are shown in Figs. 3 and 4, dem-

onstrating that the model function, Eq. (1), describes properly the time dependence of the EB field for the given time interval between 1 and 648 h after bombardment. Fit results are summarized in Table I.

Uncertainties (1σ) of the fits are less than 7%, uncertainties of individual data points are less than 5% mainly determined by uncertainties of the MOKE measurements.

Although the fluence dependencies measured at different times after IB are qualitatively similar to the fluence dependencies of other EB systems, the quantitative differences between results measured after 1 h and after 648 h at room temperature are considerable. Therefore, for a quantitative analysis of such data it is absolutely necessary to consider the temporal change in H_{EB} with time and with temperature as a parameter.

IV. MODEL CONSIDERATIONS

Many different models of the EB effect have been proposed [see, e.g., the review[18]] explaining various aspects of EB. However, a general model is still missing due to the complexity of the phenomenon. The temporal change in H_{EB} after IB can be understood as a thermal relaxation process, much alike the thermal after effect[5,6,22] for EB systems. The first quantitative theory has been proposed in 1972,[13] where it has been assumed that the EB system consists of an ensemble of noninteracting antiferromagnet (AF) particles or grains with net uncompensated magnetic moments per AF particle at the interface between the AF and the ferromagnet (FM). These AF interface moments are in exchange contact with the interface moments of a single domain FM. The magnetic part of the free energy E_i of the average uncompensated net AF interface moment i (in the following denoted as coupling site) as a function of its angle ϕ_i with respect to the AF easy axis (assumed to be parallel to the FM easy axis) is described by
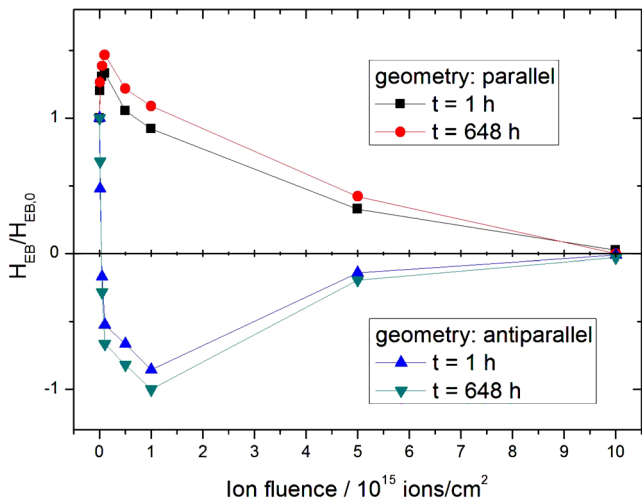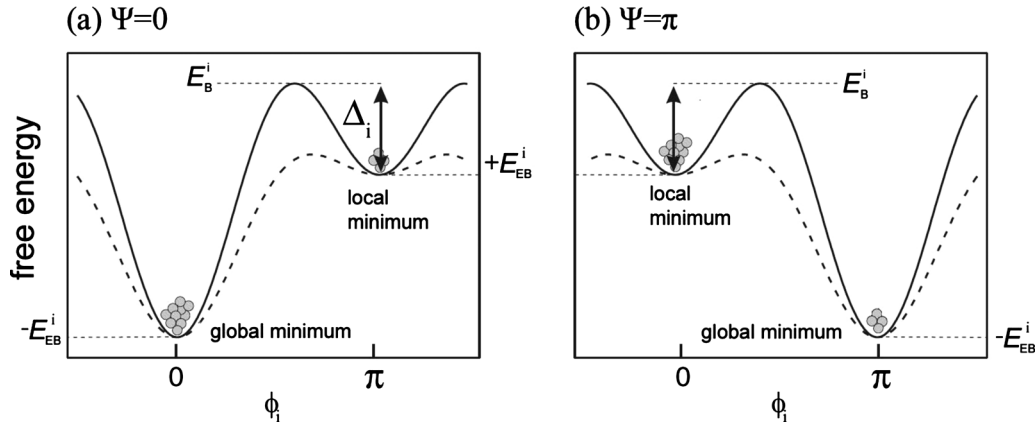

FIG. 5. (Color online) Ion fluence dependence of the normalized EB field for parallel and antiparallel field geometries measured 1 and 648 h after IB.

FIG. 6. Two-level-model adapted from Ref. [13]: Free energy per grain i as a function of the angle between pinned uncompensated AF interface moment and FM magnetization direction with unidirectional anisotropies at $\Psi = 0$ (a) and at $\Psi = \pi$ (b). The dashed line shows the free energy of a grain with half the magnetocrystalline anisotropy energy as compared to the one corresponding to the solid line.

$$E_i = K_{AF,i} \cdot S_i \cdot t_i \sin^2(\phi_i) - \kappa_{EB,i} \cdot S_i \cos(\phi_i - \psi)$$
$$= E_{AF,i} \sin^2(\phi_i) - E_{EB,i} \cos(\phi_i - \psi). \qquad (2)$$

This function displays a local and a global minimum (see Fig. 6), separated by a potential energy barrier (from the local to the global minimum) of

$$\Delta E_i^{loc \to glo} = \frac{(2E_{AF,i} - E_{EB,i})^2}{4E_{AF,i}} = E_{AF,i}\left(1 + \frac{E_{EB,i}^2}{4E_{AF,i}^2}\right) - E_{EB,i}, \qquad (3)$$

as long as $2E_{AF,i} > E_{EB,i} > 0$. The energy barrier from the global to the local minimum amounts to

$$\Delta E_i^{glo \to loc} = \frac{(2E_{AF,i} + E_{EB,i})^2}{4E_{AF,i}} = E_{AF,i}\left(1 + \frac{E_{EB,i}^2}{4E_{AF,i}^2}\right) + E_{EB,i}. \qquad (4)$$

The first part of Eqs. (3) and (4) can be defined as (cf. Fig. 6)

$$E_{B,i} = E_{AF,i}\left(1 + \frac{E_{EB,i}^2}{4E_{AF,i}^2}\right).$$

In Eqs. (2)–(4) S_i and t_i denote the AF grain's interface area to the ferromagnet and its thickness. $K_{AF,i}$ is the local AF anisotropy energy volume density averaged over the AF grain, $\kappa_{EB,i}$ the exchange coupling energy area density averaged over the interface area of the AF grain, and ψ is the angle between FM magnetization direction and FM easy axis (in the following assumed to be 0). Function (2) is exemplarily displayed in Fig. 6 for one coupling site and for two different AF magnetocrystalline anisotropy energies $E_{AF,i}$ while keeping the exchange coupling energy area density constant. For the lower AF magnetocrystalline anisotropy energy the energy barrier between the two minima is lower. Equations (3) and (4) are consistent with expressions for the energy barrier described in Refs. 19 and 20 as long as $2E_{AF,i} \gg E_{EB,i}$.

For a polycrystalline AF-layer consisting of N_{2m} identical grains not interacting with each other, the N_{2m} identical coupling sites (characterized by a grain volume averaged local AF anisotropy constant, grain volume, and grain contact

area averaged exchange coupling constant) contributing to the EB are distributed among the two minima according to

$$\frac{N^{loc}(t)}{N_{2m}} + \frac{N^{glo}(t)}{N_{2m}} = 1, \qquad (5)$$

where $N^{loc}(t)$ and $N^{glo}(t)$ are the number of coupling sites in the local and global minimum, respectively. Equation (5) holds for all times. Following[13] the number of coupling sites in the global minimum for $t \to \infty$ (i.e., in equilibrium) amounts to

$$\frac{N^{glo}(t \to \infty)}{N_{2m}} = \left[1 + \exp\left(-\frac{2E_{EB}}{k_B T}\right)\right]^{-1}, \qquad (6)$$

where k_B is Boltzmann's constant and T is the temperature. Since usually $2E_{EB} \gg k_B T_R$ (T_R room temperature), the left hand side of Eq. (6) approaches almost 1 in very short times. For the present experiments this condition is fulfilled by starting to determine the EB field 1 h after its modification by IB, therefore only small deviations of $N^{glo}(t)$ from 1 and of $N^{loc}(t)$ from 0 are expected. This leads to a simplified expression for the time dependence of the numbers of coupling sites in the global minimum as follows:[5]

$$\frac{N^{glo}(t)}{N_{2m}} = 1 - \frac{N^{loc}(t = 1\ h)}{N_{2m}} \cdot \exp\left(-\frac{t}{\tau}\right), \qquad (7)$$

where

$$\frac{1}{\tau} = \nu_0 \left[\exp\left(-\frac{\Delta E^{loc \to glo}}{k_B T}\right) + \exp\left(-\frac{\Delta E^{glo \to loc}}{k_B T}\right)\right]$$
$$\approx \nu_0 \exp\left(-\frac{\Delta E^{loc \to glo}}{k_B T}\right) \qquad (8)$$

is the reciprocal of the characteristic time for thermal relaxation of one coupling site. ν_0 is the characteristic transition rate for a spin flip which is usually assumed to be 10^9 s^{-1}.[13] If the two energy barriers differ considerably the second term of the right hand side of Eq. (8) may be neglected, resulting in the simplified expression for $1/\tau$ of the second line of Eq. (8).

In polycrystalline layers, however, there are no identical coupling sites rather than a distribution of grain volume av-
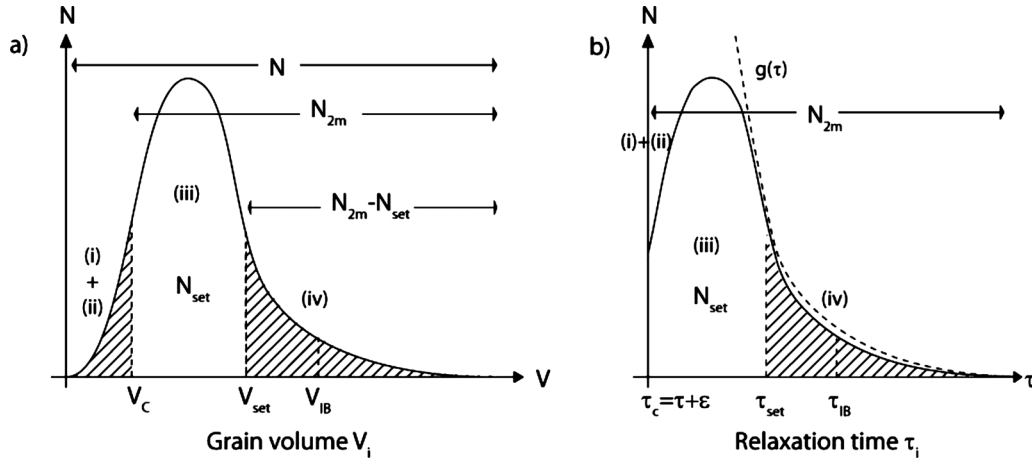
FIG. 7. Schematic grain volume distribution function (a) and relaxation time distribution function (b). Please note that the number of grains in classes (i) +(ii) of the grain volume distribution function corresponds to the number of grains at $\tau=0$ in the relaxation time distribution function. The solid line in (b) represents the schematic distribution function, the dashed line the approximation $g(\tau)$ according to Eq. (13) and Ref. 5.

eraged local AF anisotropy constants, grain volumes, and AF grain contact area averaged exchange coupling constants. This leads to a distribution of energy barriers, and, therefore, to a distribution of relaxation times. Figure 7 shows schematically two grain distribution functions, where in Fig. 7(a) the distribution is expanded over grain volumes as in Ref. 21 and in Fig. 7(b) the distribution is expanded over relaxation times. Coupling sites may be classified according to the magnitudes of the quantities entering the expression for the energy barrier[14,21] into following four groups: (i) AF grains with $k_B T_R > E_{AF,i}$; these are superparamagnetic and do neither contribute to the macroscopic EB field nor to the coercive field. (ii) $k_B T_R < E_{AF,i} < E_{EB,i}/2$; for these coupling sites there is no energy barrier between local and global free energy minimum. The exchange coupling between average uncompensated AF interface moment and ferromagnetic moment is stronger than the AF anisotropy. Therefore these coupling sites contribute to an enhanced coercive field but not to the macroscopic EB field. (iii) $kT_{set} \approx \Delta E > k_B T_R$ ($2E_{AF,i} > E_{EB,i}$); for these coupling sites the macroscopic EB may be set by FC or may be stabilized for room temperature by annealing at T_{set}. These grains show a thermally stable local coupling at room temperature and contribute to the macroscopic EB field. (iv) High energy barrier coupling sites, i.e., sites with $\Delta E \gg kT_{set}$ ($2E_{AF,i} > E_{EB,i}$): the energy barrier is high enough so that grains either in the global or in the metastable local energy minimum (see Fig. 6) remain there even at annealing temperatures T_{set} and even more so at room temperature T_R. Their local coupling cannot be modified by FC or annealing and therefore will display the original statistical local coupling distribution. These groups are indicated in the schematic distribution functions of Fig. 7. Whereas for the distribution function N(V) the integral over all volumes V results in the total number of AF grains N [Eq. (9)], the integral over τ from $\tau_c = 0+\varepsilon$ to infinity for N(τ) yields only the number of grains N_{2m}, for which $2E_{AF,i} > E_{EB,i} > 0$, i.e., the number of grains, where there are two minima in the free energy function [Eq. (10)] [number of grains in groups (iii) and (iv) above]. This corresponds to the integral from V_c to infinity using the distribution function

over V. $(N - N_{2m})$ therefore corresponds to the number of grains of groups (i) and (ii) not contributing to the macroscopic EB field. For better comparability to Ref. 21 we define the number of grains between the two volumes V_c and V_{set} as N_{set} [Eq. (9)], which corresponds to the number of grains between $\tau_c = 0+\varepsilon$ and τ_{set},

$$\int_0^\infty N \cdot f(V) dV = N,$$

$$\int_{V_c}^\infty N \cdot f(V) dV = N_{2m},$$

$$\int_{V_c}^{V_{set}} N \cdot f(V) dV = N_{set}, \qquad (9)$$

$$\int_{0+\varepsilon}^\infty N_{2m} \cdot g(\tau) d\tau = N_{2m},$$

$$\int_{0+\varepsilon}^{\tau_{set}} N_{2m} \cdot g(\tau) d\tau = N_{set}, \qquad (10)$$

$(N_{2m} - N_{set})$ corresponds to the number of coupling sites which cannot be set thermally at the setting temperature T_{set} due to their large energy barrier. In Eqs. (9) and (10) f(V) and $g(\tau)$ are normalized distribution functions. The time dependence of the EB field may therefore be described by

$$-H_{EB}(t) = \frac{\bar{\kappa}_{EB}}{\mu_0 M_{FM} d_{FM}} \cdot \int_{0+\varepsilon}^\infty [N^{glo}(t;\tau)$$
$$- N^{loc}(t;\tau)] g(\tau) d\tau$$
$$= \frac{\bar{\kappa}_{EB}}{\mu_0 M_{FM} d_{FM}} \int_{0+\varepsilon}^\infty [2N^{glo}(t,\tau) - N_{2m}] g(\tau) d\tau,$$

$$(11)$$

where $\bar{\kappa}_{EB}$ is the grain contact area averaged exchange coupling constant averaged over all grains, M_{FM} and d_{FM} the

saturation magnetization and thickness of the ferromagnet. Inserting Eq. (7) results in

$$
-H_{EB}(t) = \frac{\bar{\kappa}_{EB}}{\mu_0 M_{FM} d_{FM}} \cdot \int_{0+\varepsilon}^{\infty} \left[N_{2m} - N^{loc}(t = 1 \ h) \right.
$$
$$
\left. \cdot \exp\left(-\frac{t}{\tau}\right) \right] g(\tau) d\tau
$$
$$
= \frac{\bar{\kappa}_{EB}}{\mu_0 M_{FM} d_{FM}} \left\{ N_{2m} - \int_{0+\varepsilon}^{\infty} \left[N^{loc}(t = 1 \ h) \right. \right.
$$
$$
\left. \left. \cdot \exp\left(-\frac{t}{\tau}\right) \right] g(\tau) d\tau \right\}. \tag{12}
$$

The first term in Eq. (12) is the theoretically achievable maximum EB field $H_{EB,max}$, where all grains with two free energy minima contribute to the macroscopic EB field and all grains are aligned in the same direction. For an analytic evaluation of the integral in Eq. (12) Ref. 5 introduced a hyperbolic distribution function $g(\tau)$, forcing its normalizability by introducing two defined boundaries τ_{min} and τ_{max} according to

$$
\int_{\tau_{min}}^{\tau_{max}} g(\tau) d\tau = \int_{\tau_{min}}^{\tau_{max}} \frac{c}{\tau} d\tau = 1, \ \ \text{with} \ \ c = \left[\ln \frac{\tau_{max}}{\tau_{min}} \right]^{-1}. \tag{13}
$$

For times t obeying the conditions $t/\tau_{min} \to \infty$ and $t < \tau_{max}$ (i.e., $\tau_{min} \ll t < \tau_{max}$), the expression for the EB field may be further evaluated as follows:

$$
-H_{EB}(t) = \frac{\bar{\kappa}_{EB}}{\mu_0 M_{FM} d_{FM}} \left\{ N_{2m} - c \cdot \int_{\tau_{min}}^{\tau_{max}} [N^{loc}(t = 1 \ h)] \right.
$$
$$
\left. \cdot \frac{\exp\left(-\frac{t}{\tau}\right)}{\tau} d\tau \right\}
$$
$$
= \frac{\bar{\kappa}_{EB}}{\mu_0 M_{FM} d_{FM}} \left[N_{2m} - c \cdot N^{loc}(t = 1 \ h) \right.
$$
$$
\left. \cdot \left(-\gamma - \ln \frac{t}{\tau_{max}} \right) \right]
$$
$$
:= H_{EB,0}[h + \Delta h \ln(t)], \tag{14}
$$

where

$$
h = \frac{\bar{\kappa}_{EB}}{H_{EB,0} \mu_0 M_{FM} d_{FM}} [N_{2m} + N^{loc}(t = 1 \ h)
$$
$$
\cdot c \cdot (\gamma - \ln \tau_{max})],
$$

$$
\Delta h = -\frac{\bar{\kappa}_{EB}}{H_{EB,0} \mu_0 M_{FM} d_{FM}} \cdot N^{loc}(t = 1 \ h) \cdot c, \tag{15}
$$

and γ is the Euler–Mascheroni constant. The distribution function seems to approximate, Eq. (5), the distribution of the relaxation times for a time interval between τ_{min} and τ_{max}. The derivation of Eq. (14) also necessitates $\ln(\tau_{max}/t) > \gamma$.

From Eqs. (14) and (15) the coefficient of ln(t) determines the slope of the half logarithmic plots of Figs. 3 and 4. Therefore it is worthwhile to investigate how the relevant quantities grain volume, AF anisotropy, and exchange coupling constants enter into this expression. Inserting the expression for c and therein the simplified expression (8) for τ results in

$$
\Delta h = -\frac{N^{loc}(t = 1 \ h) \cdot \bar{\kappa}_{EB}}{\mu_0 M_{FM} d_{FM}} \cdot \frac{1}{\ln \tau_{max} - \ln \tau_{min}}
$$
$$
= -\frac{N^{loc}(t = 1 \ h) \cdot \bar{\kappa}_{EB}}{\mu_0 M_{FM} d_{FM}} \cdot \frac{k_B T \ln \nu_0}{(\Delta E_{min}^{loc \to glo} - \Delta E_{max}^{loc \to glo})} \cdot \tag{16}
$$

Approximating further that the local AF anisotropy constant is independent of the grain volume (represented by an anisotropy constant $\bar{K}_{AF}$ averaged over all grains) and approximating Eq. (3) for $2E_{AF,i} \gg E_{EB,i}$ finally yields

$$
\Delta h = -\frac{N^{loc}(t = 1 \ h) \cdot \bar{\kappa}_{EB}}{\mu_0 M_{FM} d_{FM}} \cdot \frac{k_B T \ln \nu_0}{\bar{K}_{AF}(V_{min} - V_{max})}. \tag{17}
$$

Equation (17) has been derived with several approximations, influencing its range of validity. Particularly the implicit assumption that all coupling site minima are aligned along one axis may be nonrealistic. Effects of this aspect, however, will be discussed in a separate work.

V. DISCUSSION

As has been shown earlier,[8,9] light IB of EB layer systems may lead to a modification of the EB field by local hyperthermal energy transfer, by layer intermixing at the interface,[11] and by defect creation in the AF. In the present paper a sample with a thermally stable EB field has been bombarded by 10 keV He$^+$ ions and as is obvious from Figs. 2–4 this leads to a subsequent thermal drift of the originally stable EB field toward higher absolute magnitudes. Whereas the hyperthermal energy transfer of the ions in an applied magnetic field leads to an instantaneous rotation of some of the $(N_{2m} - N_{set})$ coupling sites with high energy barriers[9] and therefore to an instantaneous change in the EB field, defect creation at the interface and in the AF layer leads to a change in $\bar{\kappa}_{EB}$ and $\bar{K}_{AF}$, and therefore to a modification of the energy barrier distribution (relaxation time distribution) towards lower energy barriers (shorter relaxation times). This causes the drift of the originally stable macroscopic EB field described approximately by Eqs. (14)–(17). At a fixed temperature and for a defined FM material with fixed thickness the slopes of the plots in Figs. 3 and 4 depend according to Eq. (17) on the initial number of coupling sites in the local energy minimum after the IB (and with not too high energy barrier), on the average exchange coupling and on the average AF anisotropy constant.

First the thermal drift of the EB field after IB in parallel field geometry (see Fig. 1) will be discussed. From Table I and Fig. 3 an increase in the coefficient Δh is observed with increasing ion fluence up to 10^{15} ions/cm^2. The faster temporal change in the EB field after bombardment with increas-

ing ion fluence may have two reasons: (1) Due to an increasing defect density in the AF layer the average AF anisotropy constant is reduced, entering Eq. (17) as $1/\bar{K}_{AF}$, therefore leading to a faster temporal change at a given temperature. (2) There will be a change in the initial number of coupling sites with appropriate energy barrier in the local energy minimum by a change in the energy barrier (relaxation time) distribution after IB. The defects caused by IB shift the distribution towards lower barriers or relaxation times. Inspecting Fig. 7 it is clear that an increase or a decrease in the initial number of coupling sites depends on the value of τ_c, and whether it is smaller or larger than the maximum of the distribution function. For τ_c smaller than the maximum, the number of coupling sites in the relevant class (iii) of coupling sites increases, for τ_c larger than the maximum it decreases. If a distribution function similar to Fig. 4 of Ref. 21 is considered a decrease of the initial number of coupling sites in the local energy minimum is likely upon bombardment, which would give the opposite trend as the observed one.

The exchange coupling constant decreases with increasing ion fluence by, e.g., interface intermixing. This would, however, lead to a slower temporal change in the EB field. Therefore, for fluences up to 10^{15} ions/cm^2 the decrease of the average AF anisotropy constant and possibly an increase in the initial number of coupling sites in the local energy minimum are the dominant effects leading to faster temporal changes with increasing ion fluence. For the highest fluence Δh decreases, indicating now that the decrease in the exchange coupling constant or the decrease in the initial number of coupling sites in the local minimum outweighs the effect of the decreasing AF anisotropy constant.

In antiparallel bombardment geometry a similar tendency is observed for Δh (Fig. 4 and Table I): between 5×10^{13} and 5×10^{15} ions/cm^2 Δh is increasing with increasing fluence. Again for 5×10^{15} ions/cm^2 the coefficient is decreasing. A special case is the temporal change in the EB field upon IB in antiparallel field geometry by 10^{13} ions/cm^2. This ion fluence is not sufficient to reverse the macroscopic EB but due to the bombardment it decreases. Δh is rather high (comparable to 10^{15} ions/cm^2 bombardment in parallel field geometry). This fast EB field increase can therefore not only be caused by the reduced AF anisotropy constant due to bombardment. Since the exchange coupling constant decreases upon IB, Eq. (17) suggests that the reason for the high drift rate seems to be the larger initial number of coupling sites in the local energy minimum.

VI. CONCLUSION

In conclusion, we have performed first investigations about the temporal stability of the EB field of $Mn_{83}Ir_{17}(15 \text{ nm})/Co_{70}Fe_{30}(10 \text{ nm})$ bilayers after 10 keV He$^+$ ion bombardment at room temperature. In these experiments the EB field has been initialized to be temporally stable. After IB the EB field starts to drift and its time dependence is observed to be approximately logarithmic. The drift velocity depends on the subjected ion fluence, increasing in a certain fluence range with increasing fluence. A tentative model has been presented where this observation is explained by the decrease in the antiferromagnetic anisotropy constant due to an IB induced increase in defect density in the antiferromagnetic layer. However, this tendency is not observed for higher and lower ion fluences, where particularly the distributions of the antiferromagnetic anisotropy constants, exchange coupling constants, volumes of grains, and geometries of grains and their changes upon IB are important.

[1]W. H. Meiklejohn and C. P. Bean, Phys. Rev. **102**, 1413 (1956).
[2]W. H. Meiklejohn and C. P. Bean, Phys. Rev. **105**, 904 (1957).
[3]S. Cardoso, P. P. Freitas, C. de Jesus, P. Wei, and J. C. Soares, Appl. Phys. Lett. **76**, 610 (2000).
[4]R. C. O'Handley, *Modern Magnetic Materials: Principles and Applications* (Wiley, New York, 2000).
[5]J. Fujikata, K. Hayashi, H. Yamamoto, and M. Nakada, J. Appl. Phys. **83**, 7210 (1998).
[6]A. Paetzold and K. Röll, J. Appl. Phys. **91**, 7748 (2002).
[7]A. Paul and S. Mattauch, J. Appl. Phys. **108**, 053918 (2010).
[8]A. Ehresmann, Recent Res. Dev. Appl. Phys. **7**, 401 (2004).
[9]A. Ehresmann, D. Junk, D. Engel, A. Paetzold, and K. Röll, J. Phys. D **38**, 801 (2005).
[10]D. Engel, I. Krug, A. Ehresmann, H. Schmoranzer, A. Paetzold, K. Röll, B. Ocker, and W. Maass, J. Appl. Phys. **94**, 5925 (2003).
[11]J. Schmalhorst, V. Hoeink, G. Reiss, D. Engel, D. Junk, A. Schindler, A. Ehresmann, and H. Schmoranzer, J. Appl. Phys. **94**, 5556 (2003).
[12]V. Höink, M. Sacher, J. Schmalhorst, G. Reiss, D. Engel, D. Junk, and A. Ehresmann, Appl. Phys. Lett. **86**, 152102 (2005).
[13]E. Fulcomer and S. H. Charap, J. Appl. Phys. **43**, 4190 (1972).
[14]S. Soeya, M. Fuyama, S. Tadokoro, and T. Imagawa, J. Appl. Phys. **79**, 1604 (1996).
[15]G. Vallejo-Fernandez, T. Deakin, K. O'Grady, S. Oh, Q. Leng, and M. Pakala, J. Appl. Phys. **107**, 09D709 (2010).
[16]A. Mougin, T. Mewes, M. Jung, D. Engel, A. Ehresmann, H. Schmoranzer, J. Fassbender, and B. Hillebrands, Phys. Rev. B **63**, 060409 (2001).
[17]D. Engel, A. Kronenberger, M. Jung, H. Schmoranzer, A. Ehresmann, A. Paetzold, and K. Röll, J. Magn. Magn. Mater. **263**, 275 (2003).
[18]F. Radu and H. Zabel, Springer Tracts Mod. Phys. **227**, 97 (2008).
[19]G. Vallejo-Fernandez, T. Dimopoulos, M. Ruehrig, and K. O'Grady, J. Magn. Magn. Mater. **310**, e786 (2007).
[20]H. Xi, J. Magn. Magn. Mater. **288**, 66 (2005).
[21]G. Vallejo-Fernandez, L. E. Fernandez-Outon, and K. O'Grady, J. Phys. D **41**, 112001 (2008).
[22]L. Néel, Rev. Mod. Phys. **25**, 293 (1953).